AMERICAN SOCIETY FOR MICROBIOLOGY | Antimicrobial Agents and Chemotherapy®

EXPERIMENTAL THERAPEUTICS

Pse-T2, an Antimicrobial Peptide with High-Level, Broad-Spectrum Antimicrobial Potency and Skin Biocompatibility against Multidrug-Resistant *Pseudomonas aeruginosa* Infection

Hee Kyoung Kang,[a] Chang Ho Seo,[b] Tudor Luchian,[c] Yoonkyung Park[a,d]

[a]Department of Biomedical Sciences, Chosun University, Gwangju, Republic of Korea
[b]Department of Bioinformatics, Kongju National University, Kongju, Republic of Korea
[c]Department of Physics, Alexandru I. Cuza University, Iasi, Romania
[d]Research Center for Proteinaceous Materials, Chosun University, Gwangju, Republic of Korea

ABSTRACT Pseudin-2, isolated from the frog *Pseudis paradoxa*, exhibits potent antibacterial activity but also cytotoxicity. In an effort to develop clinically applicable antimicrobial peptides (AMPs), we designed pseudin-2 analogs with Lys substitutions, resulting in elevated amphipathic α-helical structure and cationicity. In addition, truncated analogs of pseudin-2 and Lys-substituted peptides were synthesized to produce linear 18-residue amphipathic α-helices, which were further investigated for their mechanism and functions. These truncated analogs exhibited higher antimicrobial activity and lower cytotoxicity than pseudin-2. In particular, Pse-T2 showed marked pore formation, permeabilization of the outer/inner bacterial membranes, and DNA binding. Fluorescence spectroscopy and scanning electron microscopy showed that Pse-T2 kills bacterial cells by disrupting membrane integrity. *In vivo*, wounds infected with multidrug-resistant (MDR) *Pseudomonas aeruginosa* healed significantly faster when treated with Pse-T2 than did untreated wounds or wounds treated with ciprofloxacin. Moreover, Pse-T2 facilitated infected-wound closure by reducing inflammation through suppression of interleukin-1β (IL-1β), IL-6, and tumor necrosis factor alpha (TNF-α). These data suggest that the small antimicrobial peptide Pse-T2 could be useful for future development of therapeutic agents effective against MDR bacterial strains.

KEYWORDS antimicrobial peptide, cell selectivity, membrane disruption, multidrug-resistant bacteria, wound closure

Because resistance to commonly used antibiotics is rapidly evolving, there is an urgent need for development of new types of antimicrobial agents. This makes it more important than ever to design or identify alternative classes of antimicrobial agents with new mechanisms of action that can effectively overcome drug resistance mechanisms (1, 2). Among these new agents are antimicrobial peptides (AMPs), which reportedly exhibit antimicrobial activity against a wide range of pathogens and can be used as an alternative to conventional antibiotics for treatment of multidrug-resistant (MDR) bacteria. AMPs are produced by a variety of organisms and play important roles in host defense systems and innate immunity (3, 4). Although the details of their mechanisms of action have not been fully elucidated, AMPs typically appear to act through membrane pore formation or intracellular killing (5–7).

Pseudin-2 is a 24-amino-acid AMP isolated from the skin of the frog *Pseudis paradoxa* that exhibits strong growth-inhibitory activity against Gram-negative bacteria (7, 8). In previous studies, pseudin-2 analogs with increased cationicity were found to have greater bacterial cell selectivity, while Lys18-substituted analogs also stimulated insulin secretion via a Ca^{2+}-independent pathway (9, 10). Both pseudin-2 and its

Received 31 July 2018 **Returned for modification** 4 September 2018 **Accepted** 30 September 2018

Accepted manuscript posted online 15 October 2018

Citation Kang HK, Seo CH, Luchian T, Park Y. 2018. Pse-T2, an antimicrobial peptide with high-level, broad-spectrum antimicrobial potency and skin biocompatibility against multidrug-resistant *Pseudomonas aeruginosa* infection. Antimicrob Agents Chemother 62:e01493-18. https://doi.org/10.1128/AAC.01493-18.

Address correspondence to Tudor Luchian, luchian@uaic.ro, or Yoonkyung Park, y_k_park@chosun.ac.kr.

Lys18-substituted analogs elicit strong anti-inflammatory responses in lipopolysaccharide (LPS)-stimulated cells (11). In addition, Pro11-substituted analogs that adopted bent structures exhibited enhanced bacterial cell selectivity and cell penetration (11).

Pathogenic bacterial infections of skin wounds delay healing and can even cause worsening of the wound (12). Moreover, antibiotic treatment of wound infections is becoming more difficult, as increasing proportions of infections are caused by multidrug-resistant (MDR) bacteria that form biofilms. In particular, *Pseudomonas aeruginosa* is a major causative agent in infections of chronic wounds that greatly delays wound healing (13, 14). Acute infection by this bacterium also leads to the production of proinflammatory cytokines and chemokines, such as tumor necrosis factor alpha (TNF-α), interleukin-1β (IL-1β), and IL-6 (13, 15). Ideally, skin wound treatment would alleviate inflammation through the control of related cytokines, transcription factors, and other proteins or genes as well as through elimination of the bacteria (15, 16).

In the present study, we aimed to develop peptide-based antimicrobial biomaterials using synthetic peptides to produce short but effective AMPs with high antibacterial activity and low cytotoxicity. Here, we focused on the synthesis of truncated pseudin-2 analogs against major pathogenic bacterial strains more than membrane-active pseudin-2. Furthermore, we examined the mechanisms of the truncated pseudin-2 analogs for the development of more potent antimicrobial and effective bacterium-selective truncated analogs than pseudin-2. Additionally, the *in vivo* antimicrobial activity of Pse-T2 was evaluated in a mouse wound model infected with MDR *P. aeruginosa*.

RESULTS

Design of pseudin-2 analogs. The helical wheel diagram of pseudin-2 in Fig. S1A in the supplemental material shows its amphipathicity, with hydrophobic residues on the right side and hydrophilic residues on the left. Because Gly11 and Leu18 are located on the boundary between the hydrophilic and hydrophobic sides of the amphipathic α-helix, replacement of Gly11 or Leu18 with Lys to create Pse-11G-K and Pse-18L-K, respectively, resulted in an increase in the hydrophilicity of pseudin-2 and an increase in the cationicity to +3. In addition, a pseudin-2 analog in which both Gly11 and Leu18 were replaced with Lys (Pse-11G/18L-K) synthesized to further increase the cationicity to +4. A second set of pseudin-2 analogs, Pse-Anal1 to -7, was synthesized by substituting Trp or Ser to increase hydrophobicity. In addition, truncated analogs (Pse-T1 to -4) from pseudin-2 and its Lys-substituted analogs were synthesized to create 18-residue amphipathic helices. The sequences, molecular weights (MW), net charges, hydrophobicities, Boman indices, and cytotoxicities of 100 μM peptide toward human red blood cells (hRBCs) and HaCaT cells for pseudin-2 and its analogs are listed in Table 1.

Truncated pseudin-2 analogs show antimicrobial activity comparable to those of pseudin-2 and the Lys-substituted analogs. The antimicrobial activities of the peptides against Gram-negative and Gram-positive bacteria and yeast were compared with that of melittin, which served as a reference (Table 2). The Lys-substituted analogs Pse-11G-K, Pse-18L-K, and Pse-11G/18L-K showed higher antimicrobial activity against both Gram-negative and Gram-positive bacteria than pseudin-2. In contrast, Pse-Anal5 and Pse-Anal6, two Ser-substituted analogs, had no activity against either Gram-negative or Gram-positive bacteria. The activities of the truncated analogs (Pse-T1 to -4) against Gram-positive and Gram-negative bacteria and yeast were all higher than that of pseudin-2. To demonstrate that AMPs can kill antibiotic-resistant strains, pseudin-2 and its analogs were tested against the MDR organisms *Staphylococcus aureus* (CCARM 3518 and CCARM 3940), *Escherichia coli* (CCARM 1229 and CCARM 1238), and *P. aeruginosa* (4007 and 4891). Remarkably, Pse-11G-K, Pse-Anal2, Pse-T2, and Pse-T4 showed very high potency against these pathogens, with MICs of 2 to 4 μM, and were as effective as melittin. Finally, Pse-T1 to -4 showed potent antimicrobial activities against *Candida albicans* and *Trichosporon beigelii*, which are fungal strains. Of the

TABLE 1 Amino acid sequences and properties of pseudin-2 and analog peptides[a]

Peptide	Sequence	Theoretical MW	Measured MW[b]	Net charge	*H*[c]	μH[c]	BI[d]	Hemolysis[e] (%)	Cytotoxicity[f] (%)
Pseudin-2	GLNALKKVFQGIHEAIKLINNHVQ-NH_2	2,685.8	2,685.2	2	0.407	0.547	0.73	10.01	18
Pse-11G-K	GLNALKKVFQKIHEAIKLINNHVQ-NH_2	2,756.3	2,756.1	3	0.365	0.557	1	99.17	64
Pse-18L-K	GLNALKKVFQGIHEAIKKINNHVQ-NH_2	2,700.2	2,700.1	3	0.295	0.614	1.17	36.38	19
Pse-11G/18L-K	GLNALKKVFQKIHEAIKKINNHVQ-NH_2	2,771.3	2,771.2	4	0.253	0.63	1.44	18.04	9
Pse-Anal1	WLNALKKVFQGIHEAIKLINNHVQ-NH_2	2,814.3	2,814.3	2	0.5	0.635	0.67	100	98.2
Pse-Anal2	WLNALKKVFQGIHEAIKLIWNHVQ-NH_2	2,886.4	2,886.4	2	0.619	0.644	0.3	88.57	94.9
Pse-Anal3	WLNALKKVFQGIHEAIKLIWNWVQ-NH_2	2,935.5	2,935.5	2	0.708	0.671	0.01	100	89.7
Pse-Anal4	WLNALKKVWQGIHEAIKLIWNWVQ-NH_2	2,974.5	2,974.5	2	0.727	0.681	0.04	100	89.2
Pse-Anal5	GLNALKKVSQGIHEAIKLINNHVQ-NH_2	2,625.1	2,625.1	2	0.33	0.511	1	20.08	16.5
Pse-Anal6	GLNALKKVSQGIHESIKLINNHVQ-NH_2	2,641.1	2,641.1	2	0.316	0.503	1.22	1.43	7.9
Pse-Anal7	ALNALKKVSQGIHEAIKLIANHVQ-NH_2	2,596.1	2,595.7	2	0.381	0.528	0.61	0.05	0
Pse-T1	LNALKKVFQGIHEAIKLI-NH_2	2,035.5	2,035.6	2	0.546	0.633	−0.04	12.30	13.8
Pse-T2	LNALKKVFQKIHEAIKLI-NH_2	2,106.6	2,106.6	3	0.491	0.649	0.31	15.21	18.6
Pse-T3	LNALKKVFQGIHEAIKKI-NH_2	2,050.5	2,050.5	3	0.397	0.728	0.53	5.64	9.7
Pse-T4	LNALKKVFQKIHEAIKKI-NH_2	2,121.6	2,121.7	4	0.342	0.753	0.89	1.33	3.5

[a]Underlined letters are the amino acid residues substituted in this study.
[b]Molecular weights (MW) were measured using mass spectroscopy.
[c]Hydrophilicity (*H*) and the hydrophobic moment (μH) were calculated by using HeliQuest (http://heliquest.ipmc.cnrs.fr/).
[d]BI indicates the Boman index, which represents protein-binding potential. Boman index values were determined according to the Antimicrobial Peptide Database (http://aps.unmc.edu/AP/main.php).
[e]Percent hemolysis against 100 μM peptide on hRBCs.
[f]Cytotoxicity against 100 μM peptide on HaCaT human keratinocytes.

tested peptides, Pse-T2 showed the strongest antimicrobial activity against *C. albicans* and *T. beigelii*, with MICs of 16 and 8 μM, respectively.

Additionally, we compared the time courses of *E. coli* and *S. aureus* cell viability in the presence of pseudin-2 or Pse-T1 to -4 at their respective MICs (see Fig. S1 in the supplemental material). Specifically, Pse-T2 caused a 2.34-$\log_{10}$ reduction in *E. coli* and a 1.41-$\log_{10}$ reduction in *S. aureus* cell viability (99.54% and 96.02% killing, respectively) after 15 min of treatment and complete killing by 25 and 30 min, respectively. Both strains were completely eradicated by all truncated analogs within 50 min. In contrast, the bactericidal effect of pseudin-2 was exhibited by a 2.7-$\log_{10}$ reduction in *E. coli* and a 1.91-$\log_{10}$ reduction in *S. aureus* cell viability (99.79% and 98.76% killing, respectively) after 50 min of treatment and complete killing by 70 min. In *E. coli*, the bactericidal activity of Pse-T2 and ciprofloxacin was fast (6-$\log_{10}$ reduction within 30 min) compared to that of pseudin-2 or melittin (Fig. S1A). Unlike *E. coli*, the killing of *S. aureus* by ciprofloxacin was much slower, with a reduction in the initial inoculum of only 2 $\log_{10}$ units within 80 min (Fig. S1B).

Truncation of pseudin-2 and Lys substitution reduce cytotoxicity against hRBCs and HaCaT cells. The cytotoxicity of the peptides against mammalian cells was tested by measuring their ability to cause lysis of hRBCs and by determining the survival rate of HaCaT keratinocytes. The hemolytic activities of the peptides against hRBCs are shown in Fig. 1A to D and Table 1. At a high concentration (100 μM), pseudin-2, Pse-Anal6, Pse-Anal7, Pse-T1, Pse-T2, Pse-T3, and Pse-T4 exhibited little or no hemolytic activity, while Pse-11G/18L-K and Pse-Anal5 showed moderate hemolytic activity (18.04% and 20.08%, respectively), as observed for ciprofloxacin, the reference antibiotic. In contrast, high levels of hemolysis were induced by Pse-11G-K, Pse-Anal1, Pse-Anal2, Pse-Anal3, and Pse-Anal4 (99.17%, 100%, 88.57%, 100%, and 100%, respectively). Melittin, the reference AMP, caused complete hemolysis at 50 μM.

As a result of the hemolytic action at the maximum MIC of the bacteria for each peptide, pseudin-2 (32 μM), Pse-11G/18L-K (8 μM), Pse-Anal6 (32 μM), Pse-Anal7 (16 μM), Pse-T1 (8 μM), Pse-T2 (4 μM), Pse-T3 (4 μM), Pse-T4 (4 μM), Pse-18L-K (4% in 8 μM), and Pse-Anal5 (7% in 32 μM) showed no or slight hemolytic activity. In contrast, Pse-11G-K (27.7% in 4 μM), Pse-Anal1 (82.3% in 32 μM), Pse-Anal2 (45.9% in 4 μM), Pse-Anal3 (100% in 32 μM), and Pse-Anal4 (99.6% in 32 μM) induced high levels of hemolysis at the MIC. Our data indicate that truncated pseudin-2 analogs (particularly Pse-T2) were the most effective antimicrobial agents against pathogenic bacteria.

TABLE 2 Antimicrobial activities of the peptides against microorganisms

Microorganism	MIC (μM)[a]																
	Pseudin-2	Pse-11G-K	Pse-18L-K	Pse-11G/18L-K	Pse-Anal1	Pse-Anal2	Pse-Anal3	Pse-Anal4	Pse-Anal5	Pse-Anal6	Pse-Anal7	Pse-T1	Pse-T2	Pse-T3	Pse-T4	Melittin	Ciprofloxacin
Gram-positive organisms																	
S. aureus ATCC 25923	32	4	8	8	32	4	32	32	32	32	16	8	4	4	4	2	2
Bacillus subtilis KCTC 1998	32	4	8	8	32	4	32	32	32	32	16	8	4	4	8	1	2
Listeria monocytogenes KCTC 3710	32	8	8	8	32	8	32	32	32	32	16	8	4	8	8	4	4
Gram-negative organisms																	
E. coli ATCC 25922	16	2	4	4	16	2	16	16	16	16	8	4	2	2	2	2	0.25
P. aeruginosa ATCC 27853	16	2	2	2	16	2	16	16	16	16	8	4	2	4	4	4	0.5
Salmonella enterica serovar Typhimurium KCTC 1926	16	2	4	4	16	2	16	16	16	16	8	4	2	4	4	4	0.75
Yeast																	
C. albicans KCTC 7270	32	32	32	32	64	32	32	32	64	64	32	16	16	16	16	8	>400
T. beigelii KCTC 7707	32	32	32	32	64	32	32	32	64	64	32	16	8	16	16	4	>400
Resistant Gram-positive organisms																	
S. aureus CCARM 3518	32	4	8	4	32	4	32	32	64	64	32	8	4	4	4	2	>400
S. aureus CCARM 3090	32	4	8	8	32	4	32	32	64	64	32	8	4	4	4	2	>400
Resistant Gram-negative organisms																	
E. coli CCARM 1229	16	2	4	4	16	2	32	32	32	64	16	4	2	2	2	1	64
E. coli CCARM 1238	16	2	4	4	16	2	32	32	32	64	16	4	2	2	2	2	64
P. aeruginosa 4007	16	2	2	2	16	2	64	64	64	64	32	4	2	4	4	2	>400
P. aeruginosa 4891	16	4	8	4	16	4	64	64	64	64	32	8	4	8	4	4	>400

[a]MICs were determined in three independent experiments performed in triplicate.

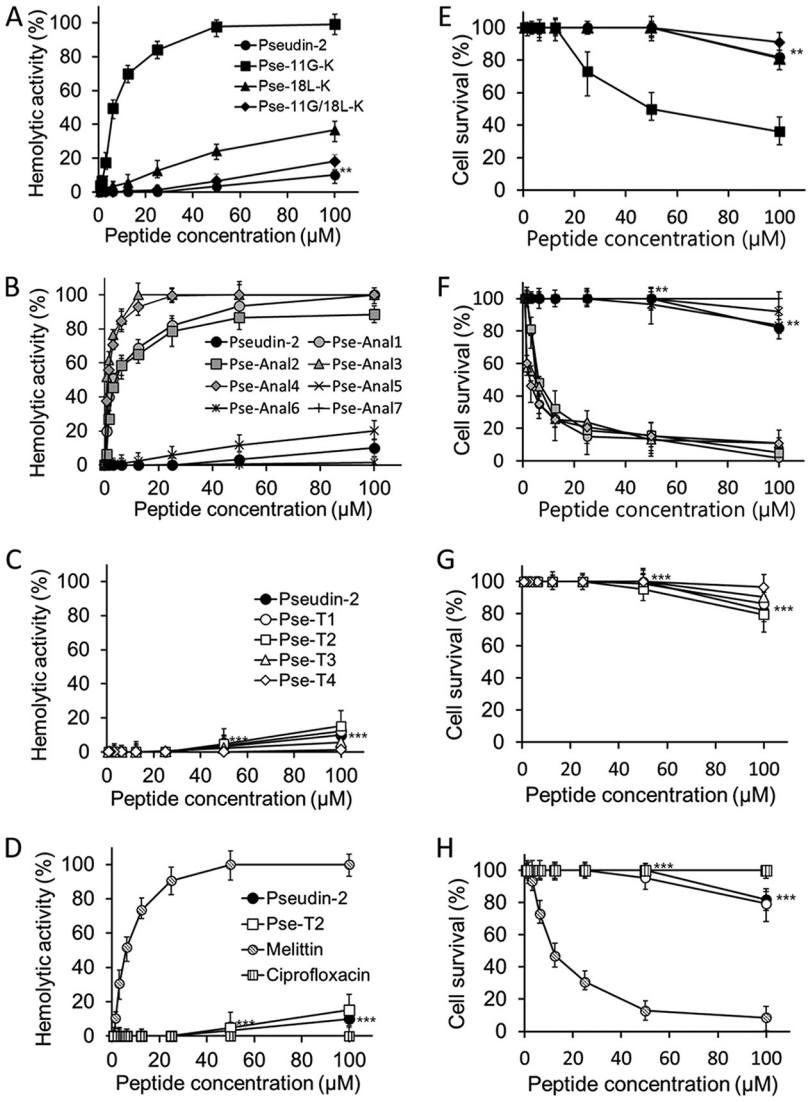

FIG 1 Hemolysis in hRBCs and cytotoxicity against HaCaT human keratinocytes. (A to D) Dose-response curves for hemolytic activity against hRBCs. (E to H) Dose-response curves for cytotoxic activity against HaCaT cells. Symbols represent means ± standard deviations from triplicate determinations. **, $P < 0.01$; ***, $P < 0.001$ (versus pseudin-2).

The cytotoxicity of the peptides against HaCaT keratinocytes cells is shown in Fig. 1E to H and Table 1. The rate of cell survival following treatment with Pse-11G-K at 100 μM was lower than that with pseudin-2, indicating that Pse-11G-K (63.7%) is more cytotoxic than pseudin-2 (11.6%). In contrast, both Pse-18L-K and Pse-11G/18L-K (18.7% and 8.8%, respectively) at 100 μM showed moderate cytotoxicity similar to that of pseudin-2 (Fig. 1E). It appears that the increased net charge of Pse-11G/18L-K resulted in higher cell survival rates than with pseudin-2. On the other hand, the survival rate among HaCaT cells exposed to Pse-11G-K was much lower than with pseudin-2, which implies that Lys11 substitution increased the peptide's cytotoxicity. Notably, survival rates among HaCaT cells exposed to 100 μM Pse-T1 to -4 were higher (86%, 80%, 90%, and 97%, respectively) than among cells exposed to the corresponding untruncated peptides (Fig. 1G), whereas survival rates among cells exposed to Pse-Anal1, Pse-Anal2, Pse-Anal3, and Pse-Anal4 were much lower (2%, 5%, 11%, and 11%, respectively). Cell survival rates were higher with all Ser-substituted analogs (Pse-Anal5, Pse-Anal6, and Pse-Anal7) than with pseudin-2 (Fig. 1F).

CD spectra of pseudin-2 and its truncated analogs in membrane-like environments. We measured circular dichroism (CD) spectra to detect the secondary structures of pesudin-2 and its truncated analogs in the presence of bacterial membrane-mimetic liposomes composed of L-α-phosphatidylethanolamine–L-α-phosphatidyl-DL-glycerol sodium salt (PE/PG) (7:3) lipids and eukaryotic membrane-mimetic liposome of phosphatidylcholine-cholesterol-sphingomyelin (PC/CH/SM) (1:1:1) (see Fig. S1C in the supplemental material). As shown in Fig. S1C (left) in the supplemental material, the spectra indicated that the peptides were unordered in aqueous solution but exhibited conformational changes in large unilamellar vesicles (LUVs) composed of PE/PG (7:3) or PC/CH/SM (1:1:1) (Fig. S1C, middle and right, respectively). Pseudin-2 and the truncated analogs adopted a significant degree of α-helical structure in all membrane-mimetic environments, as indicated by the characteristic double-negative minima at 205 nm and 220 nm in their CD spectra. Truncated analogs that contained a Lys substitution (Pse-T2, Pse-T3, and Pse-T4) showed greater α-helical content than did Pse-T1. In PC/CH/SM (1:1:1) liposomes, the peptides formed weaker secondary structures than the PE/PG (7:3) liposome. This demonstrates that pseudin-2 and its truncated analogs had different secondary structures depending on the type of liposome. Changes in the conformation/physicochemical properties of AMP will lead to different mechanisms of interaction with bacterial and eukaryotic membrane-mimetic liposomes and, thus, organism selectivity (Fig. S1B).

Mechanisms of action of pseudin-2 and its truncated analogs. We separately tested the effects of the peptides on the permeability of the outer and inner membranes of Gram-negative bacteria. To investigate outer membrane permeability, we used the hydrophobic probe *n*-phenyl-1-naphthylamine (NPN) (Fig. 2A). When the outer membrane is damaged and functionally invalid, NPN is partitioned into the disrupted outer membrane, where it exhibits increased fluorescence (17). All of the peptides induced dose-dependent increases in outer membrane permeability, as indicated by increases in NPN fluorescence (Fig. 2A). These results suggest that the permeability of the outer membrane of *E. coli* ATCC 25922 cells exposed to the truncated peptides at 0.5× MIC was more than 50% but was less than 50% in bacteria exposed to pseudin-2 at 0.5× MIC. Outer membrane permeability reached 90% at 2× MIC with Pse-T2 or 4× MIC with Pse-T1 or Pse-T3. Pse-T2 treatment showed results similar to those obtained by treatment with the pore-forming peptide melittin as a control.

Peptide-induced permeabilization of the inner membrane was detected when *o*-nitrophenyl-β-galactosidase (ONPG) entered the cytoplasm and was degraded by β-galactosidase, producing *o*-nitrophenol, which increased the absorbance at 420 nm. As shown in Fig. 2B and C, all of the peptides induced increases in the permeability of the inner membrane at 1× or 0.5× MIC. In addition, Pse-T1 to -4 all induced more inner membrane permeabilization than did pseudin-2 at these concentrations. However, the membrane perturbation activity of pseudin-2 and its analogs was weak at 2× MIC but similar to those of well-known cytotoxic and membrane-active melittin peptides at 1× MIC. This demonstrates that the peptides may use similar mechanisms of action.

Depolarization of the peptides in the *E. coli* cytoplasmic membrane was evaluated using the membrane potential-sensitive dye 3,3′-dipropylthiadicarbocyanine iodide ($DiSC_3$-5). As shown in Fig. 2D, three peptides, pseudin-2, Pse-T2, and melittin, induced dose-dependent increases in $DiSC_3$-5 fluorescence, reflecting cytoplasmic membrane depolarization. Pse-T2 caused more rapid and stronger membrane depolarization than pseudin-2 but weaker depolarization than that caused by melittin at the same molar concentrations.

To compare the abilities of the peptides to induce membrane depolarization in Gram-positive bacteria, we performed the same assays using *S. aureus* (Fig. 2E). Similar to that in the *E. coli* membrane, Pse-T2 caused stronger membrane depolarization than pseudin-2 in the *S. aureus* membrane. However, pseudin-2 and Pse-T2 induced approximately 35% less depolarization of Gram-positive *S. aureus* membranes than Gram-

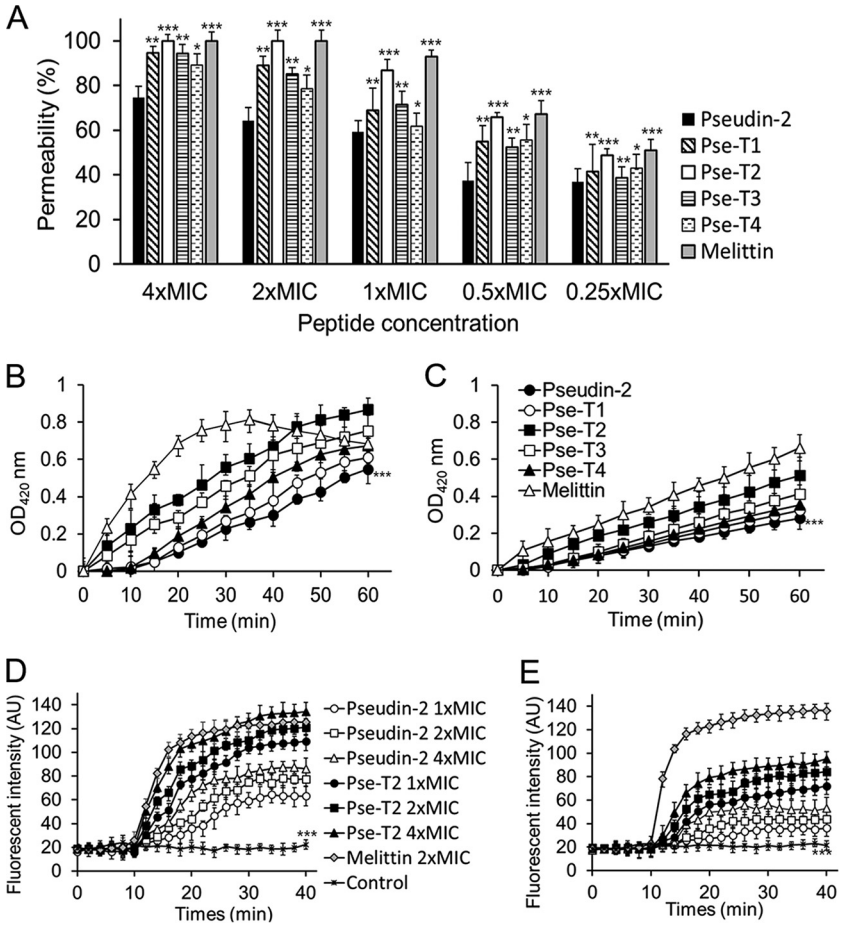

FIG 2 Effects of pseudin-2 and its truncated analogs on bacterial membrane permeability. (A) Outer membrane permeability. Shown is membrane uptake of NPN by *E. coli* ATCC 25922 in the presence of the indicated concentrations of peptide. *, $P < 0.05$; **, $P < 0.01$; ***, $P < 0.001$ (versus pseudin-2 at the same MIC). (B and C) Inner membrane permeability. Hydrolysis of ONPG due to the release of cytoplasmic β-galactosidase in *E. coli* ATCC 25922 cells treated with the indicated peptides at 1× MIC (B) or 0.5× MIC (C) was measured for 60 min at 420 nm. ***, $P < 0.001$ (versus pseudin-2). (D and E) Changes in cytoplasmic membrane potential indicated by the membrane potential-sensitive dye $DiSC_3$-5 in *E. coli* ATCC 25922 (D) and *S. aureus* ATCC 25923 (E) cells treated with pseudin-2 or Pse-T2. All data are presented as means ± standard deviations from triplicate experiments. AU, arbitrary units. ***, $P < 0.001$ versus the control.

negative *E. coli* membranes. In contrast, melittin showed similar melittin-induced depolarization kinetics in both *E. coli* and *S. aureus*.

SYTOX green uptake into the cell cytosol was examined to gain further insight into the extent to which the peptide induced membrane disruption. This cationic dye will not enter the cell without disruption of the inner membrane, and its fluorescence increases upon binding to cytoplasmic nucleic acids. Pseudin-2 and its truncated analogs all elicited dose-dependent increases in SYTOX fluorescence, with Pse-T2 having the greatest effect compared to the negative control (without peptide) (Fig. 3A to C). Melittin as a positive control induced rapid permeabilization, with maximum SYTOX green influx being reached by 20 min compared to the influx of 85% observed for Pse-T2 at 4× the MIC. Consistent with its bactericidal activity against *E. coli*, Pse-T2 induced membrane permeabilization within about 30 min (Fig. 3A to C). This suggests that the bactericidal effect of Pse-T2 on *E. coli* is mediated directly through membrane permeabilization, which exhibits kinetics similar to its killing kinetics (see Fig. S2 in the supplemental material).

Surface disruption and internalization of pseudin-2 and its truncated analogs. Flow cytometry was employed to further characterize the mechanism of action of the

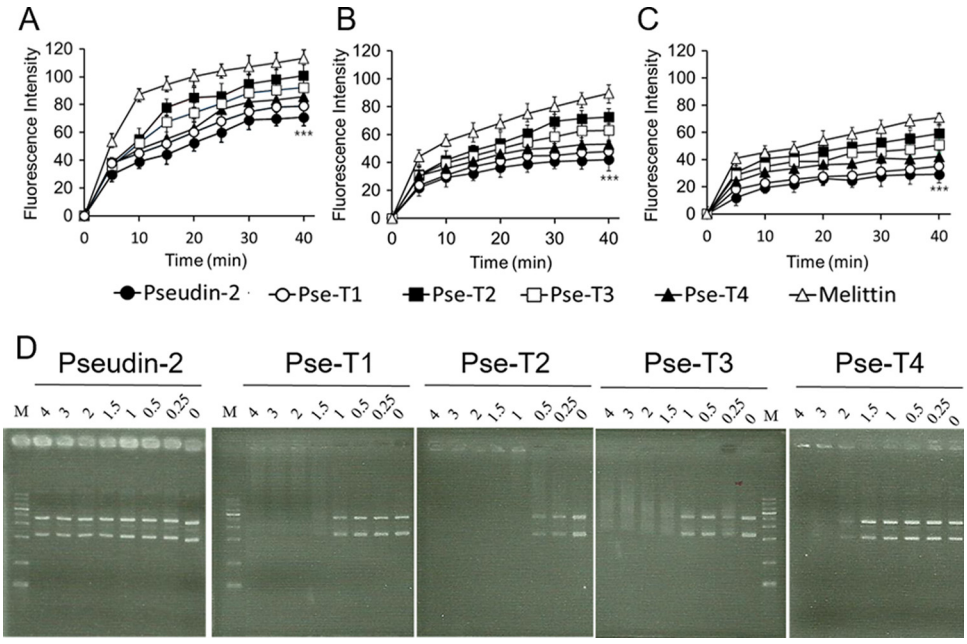

FIG 3 Bactericidal mechanism of pseudin-2 and its truncated peptides. (A to C) SYTOX green uptake into *E. coli* ATCC 25922 cells treated with the indicated peptides at 4× MIC (A), 2× MIC (B), and 1× MIC (C). Fluorescence was measured at the indicated times (excitation wavelength at 485 nm and emission wavelength at 520 nm). Symbols are the means ± standard deviations. ***, $P < 0.001$ versus pseudin-2 at the highest concentration. (D) DNA binding activity of pseudin-2 and its truncated analogs. The peptide was mixed for 10 min with pRSET A plasmid DNA at the indicated peptide/DNA ratio. The mobility of the DNA was determined in gel retardation assays. Peptide/DNA ratios are shown at the top.

peptides. We found that after treatment with the peptides at their respective MICs, fluorescent signals indicating the uptake of propidium iodide (PI) were significantly increased (Fig. 4), which is indicative of membrane disruption. Pse-T1 (75%), Pse-T2 (92%), Pse-T3 (34%), and Pse-T4 (75%) all induced greater disruption of membrane integrity in *E. coli* ATCC 25922 cells than did pseudin-2 (34%). In addition, pseudin-2 induced membrane damage in 48% of *S. aureus* ATCC 25923 and MDR *P. aeruginosa* 4891 cells (Fig. 4 and Fig. S3). Pse-T2 exhibited the highest potential to damage *E. coli* ATCC 25922 (92%), *S. aureus* ATCC 25923 (96%), and *P. aeruginosa* 4891 (70%).

Truncated analogs bind to bacterial DNA, but pseudin-2 does not. Peptide binding to intracellular DNA was detected as a shift in the plasmid DNA bands upon electrophoresis. The strongest effect was seen with Pse-T2, which first elicited a DNA band shift at a peptide/DNA weight ratio of 0.25, and a complete retardation of the DNA, which indicates aggregation of the DNA with Pse-T2, was seen at a weight ratio of 1 (Fig. 3D). In contrast, pseudin-2 had no effect on the migration of plasmid DNA, even at a peptide/plasmid DNA weight ratio of 4, which indicates that pseudin-2 does not bind to DNA.

Visualization of the interaction of pseudin-2 and its truncated analogs with *E. coli* and *S. aureus*. Scanning electron microscopy (SEM) was used to directly visualize bacterial membrane damage following treatment with peptides. Figure 5 shows images of *E. coli* and *S. aureus* cells treated for 30 min with pseudin-2 or Pse-T1 to -4 at their respective MICs. Untreated control cells have bright, smooth surfaces, whereas treated cells exhibited significant membrane damage. The surface of *E. coli* cells treated with Pse-T2 or Pse-T3 was rougher and had more blebbing than that of cells treated with pseudin-2 (Fig. 5A). Cell surfaces exposed to the peptides gave the appearance of being perforated and blistered, with leakage of cytoplasmic contents observed in some cases. Similar peptide-induced changes were observed in *S. aureus* cells, with Pse-T1 and Pse-T4 inducing substantially greater roughening and blebbing of the cell membrane than pseudin-2. Distortion and blebbing or breakage of the cell membrane was also evident in cells treated with Pse-T2 or Pse-T3 (Fig. 5B).

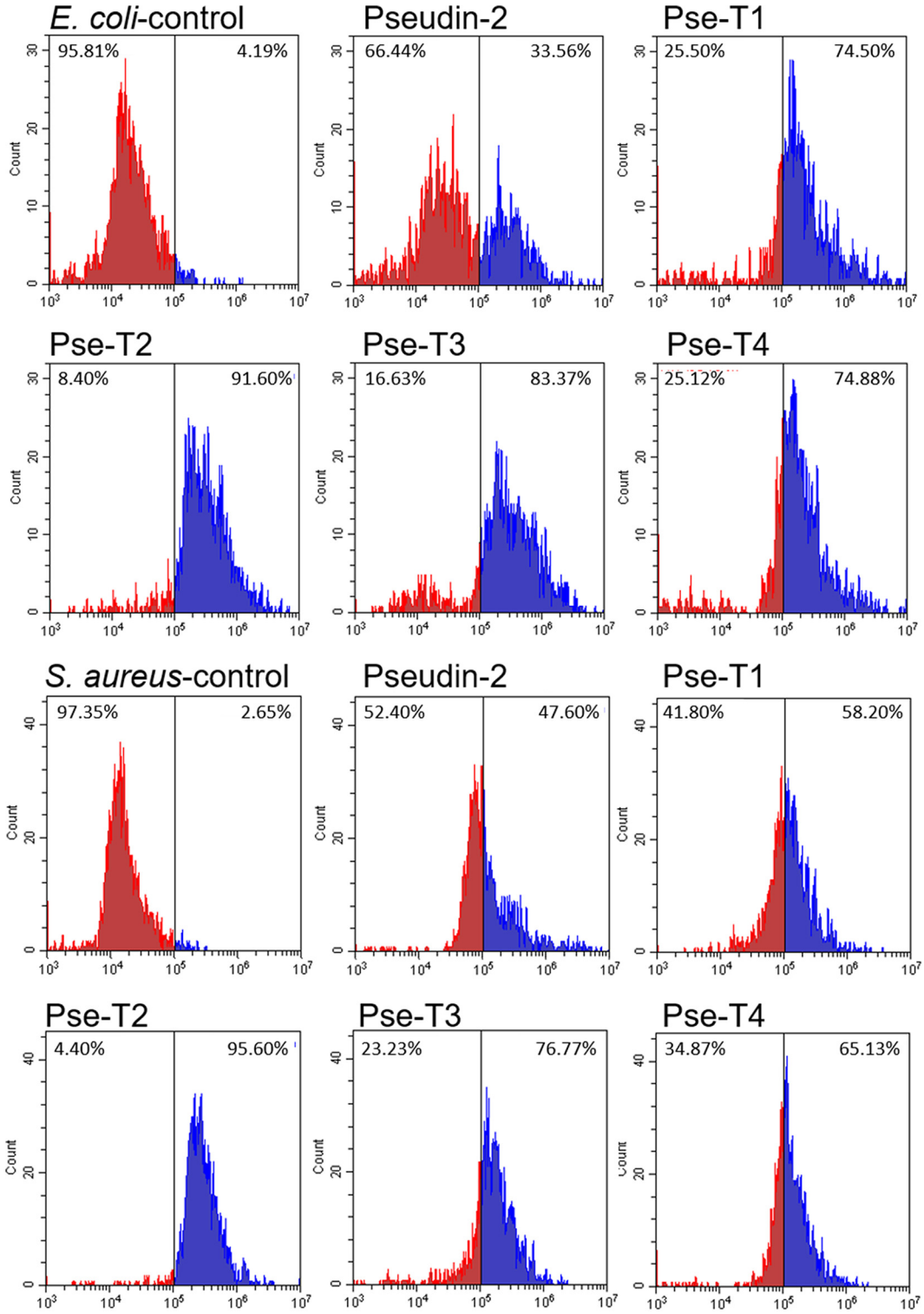

FIG 4 Membrane permeabilization detected as an increase in PI fluorescence in *E. coli* ATCC 25922 and *S. aureus* ATCC 25923 cells treated with peptides for 1 h. The control was done without peptides.

Pseudin-2 and its truncated analogs induce leakage from LUVs. To further investigate the mechanism of action of the peptides, we assessed changes in membrane permeability by measuring the release of the fluorescent marker calcein (MW, 623; diameter, 1 nm) from LUVs with lipid compositions that mimic those of the

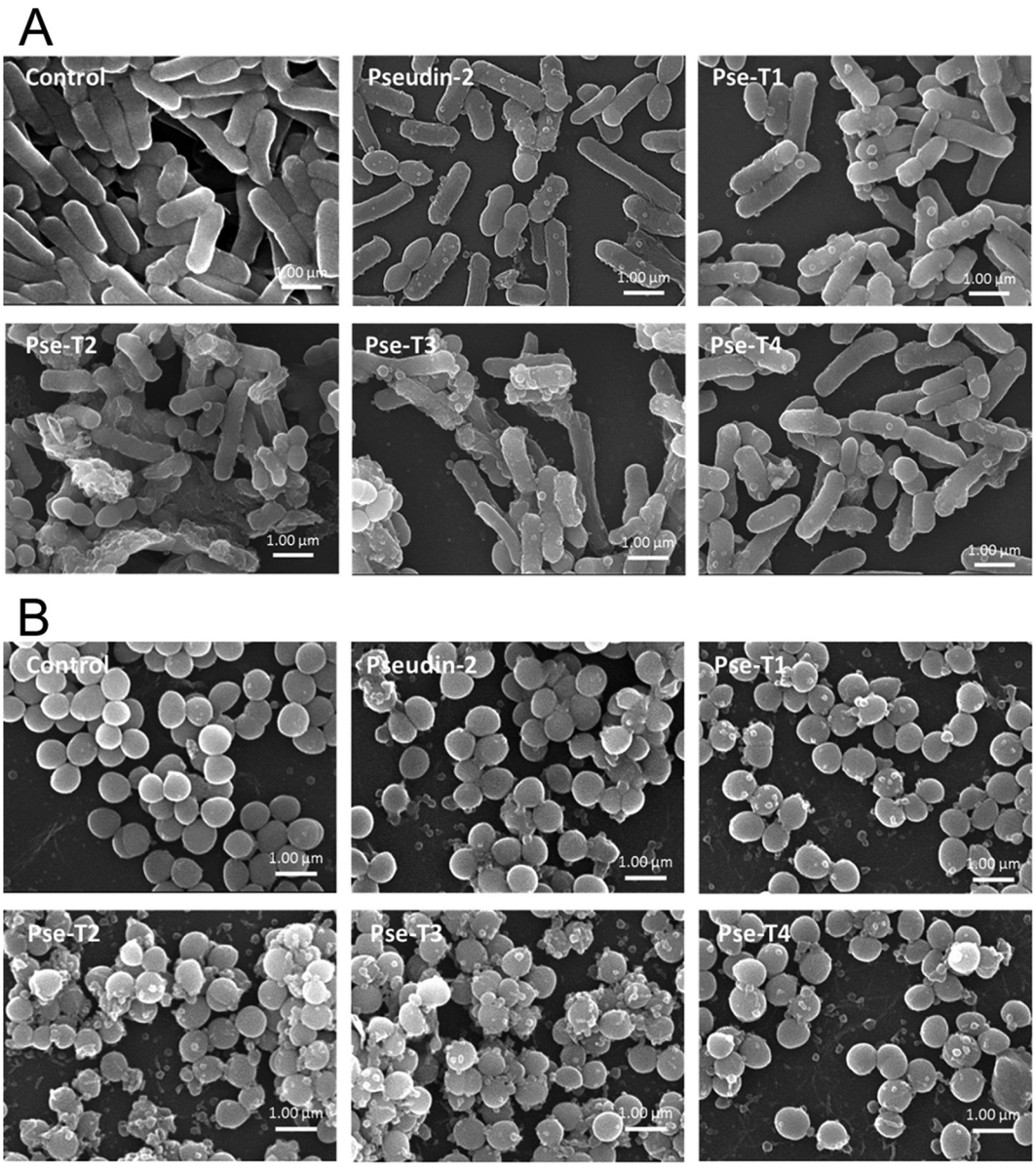

FIG 5 Scanning electron micrographs of *E. coli* ATCC 25922 (A) and *S. aureus* ATCC 25923 (B) treated with the indicated peptides at 1× MIC for 30 min. The control was performed without peptides.

membranes of Gram-negative bacteria and hRBCs. We used LUVs with a 7:3 (wt/wt) ratio of PE/PG to mimic the membrane of Gram-negative *E. coli* and those with a 1:1:1 (wt/wt/wt) ratio of PC/CH/SM to mimic hRBC membranes. Figure S4 in the supplemental material shows the concentration-response curves for peptide-induced calcein release. Truncated peptides induced 92 to 98% dye leakage from PE/PG vesicles at a peptide-to-lipid molecular ratio (P/L ratio) of 0.1, which was higher than that of the parental peptide pseudin-2. The pore-forming peptide melittin was used as a control and was found to induce nearly 100% leakage at a P/L ratio of 0.05. Even at a P/L ratio of 0.2, the truncated peptides caused leakage (61 to 69%) only in the zwitterionic membrane of PC/CH/SM vesicles, unlike PE/PG vesicles (92 to 98%). The relative abilities of the peptides to induce leakage from PE/PG vesicles coincided well with their bactericidal activities against Gram-negative bacteria. The peptides were less effective at inducing leakage from PC/CH/SM vesicles mimicking hRBC membranes, implying that they are bacterial cell selective. These results showed that the relative abilities of

the peptides to induce leakage from zwitterionic vesicles are consistent with their relative hemolytic activities and cytotoxicities. Because the truncated analogs more effectively permeabilized all membranes while exhibiting much less cell cytotoxicity than Lys-substituted peptides (Fig. 1), we selected truncated peptides, especially Pse-T2, as potential candidate peptide antibiotics.

Some AMPs insert into the cytoplasmic membrane after pore formation, resulting in dissipation of the membrane potential and destruction of the lipid asymmetry, leading to cell death (18). In previous reports, pseudin-2 was found to form pores upon interaction with the membrane in both bacterial cells and artificial vesicles (7). To estimate the size of the membrane defects caused by pseudin-2 and Pse-T1 to -4, release of fluorescein isothiocyanate (FITC)-dextrans from PE/PG (7:3, wt/wt) and PC/CH/SM (1:1:1, wt/wt/wt) LUVs was investigated (Fig. S5). The release of encapsulated markers by pseudin-2 and its truncated analogs was strongly dependent on the marker size. Pse-T2 at 10 μM (P/L ratio of 0.2) induced the release of 100% of fluorescein isothiocyanate-dextran 4 (FD4; MW, 3.9 kDa; diameter, 2.8 nm) and 94% of FD10 (9.9 kDa; 4.6 nm) from PE/PG LUVs but only 35% of FD20 (19.8 kDa; 6.6 nm) and 29% of FD40 (40.5 kDa; 9 nm) (Fig. S5A to Fig. S5D). At the same concentration, Pse-T2 released 84% of FD4 but only 17% of FD40 from PC/CH/SM LUVs (Fig. S5E to Fig. S5H). The pores induced by 10 μM (P/L ratio of 0.2) pseudin-2 or its truncated analogs thus have apparent diameters of between 2.8 and 6.6 nm.

Salt resistance of pseudin-2 and its truncated analogs. Because the activities of some AMPs are known to be affected by the ionic strength of their environment, we investigated the effects of cations on the activities of the peptides (19). We found that in the presence of 300 mM Na^+, there was a slight reduction in the antibacterial activities of pseudin-2 and its truncated analogs against *P. aeruginosa* 4891 (see Fig. S6A in the supplemental material). Overall, pseudin-2 was more affected by the addition of monovalent cations than the truncated analogs. The addition of divalent cations ($Ca^{2+}$and Mg^{2+}) also reduced the efficacy of the peptides against *P. aeruginosa* 4891. The presence of Ca^{2+} resulted in a slight reduction of the antimicrobial activity of pseudin-2 and its truncated analogs, which retained 54% to 75% of their antibacterial activity, even at 5 mM Ca^{2+}. However, Mg^{2+} had a somewhat stronger repressive effect on the antibacterial activity of the peptides than either Na^+ or Ca^{2+}.

Pse-T2 inhibits biofilm formation by MDR bacteria. Biofilms may form on living or nonliving surfaces and can play a major role in infections by reducing responsiveness to antibiotics. To assess the biofilm susceptibility of Pse-T2, we tested its ability to inhibit biofilm formation by *P. aeruginosa* (ATCC 27853 and 4891), *E. coli* (ATCC 25922 and CCARM 1238), and *S. aureus* (ATCC 25923 and CCARM 3090) on plastic. All the strains formed extensive biofilms in the absence of Pse-T2 (Fig. 6A). The maximum percentages of biofilm inhibition by Pse-T2 were 99.3% against *P. aeruginosa* ATCC 27853, 99.2% against *E. coli* ATCC 25922, and 99.4% against *S. aureus* ATCC 25923 (Fig. 6B). In addition, it was confirmed that Pse-T2 effectively inhibits biofilm formation by MDR strains (97% against *P. aeruginosa* 4891, 89.8% against *E. coli* CCARM 1238, and 94.2% against *S. aureus* CCARM 3090) (Fig. 6C). We also determined the minimal biofilm inhibition concentrations (MBICs) against MDR *S. aureus*, *E. coli*, and *P. aeruginosa*. At concentrations of 8 to 32 μM, Pse-T2 inhibited biofilm formation (Table 3). These results clearly demonstrate that Pse-T2 inhibits biofilm formation. Based on these results, the effect of Pse-T2 on *P. aeruginosa* 4891 was assessed *in vivo*.

Pse-T2 enhances closure of *P. aeruginosa* 4891-infected wounds. We next assessed the efficacy of Pse-T2 *in vivo* using a mouse model. After abrading the skin on the backs of BALB/c mice, we injected 10^8 CFU of *P. aeruginosa* 4891 into the wounded skin (Fig. 7A). In the absence of *P. aeruginosa* 4891 infection, wounds injected with phosphate-buffered saline (PBS), Pse-T2, or ciprofloxacin all completely closed within 6 to 8 days (Fig. 7A and B and Fig. 8B). Three days after injury, *P. aeruginosa* 4891-infected wounds were larger than wounds without infection. Indeed, the sizes of infected wounds had not decreased after 2 weeks, by which time the wounds had become

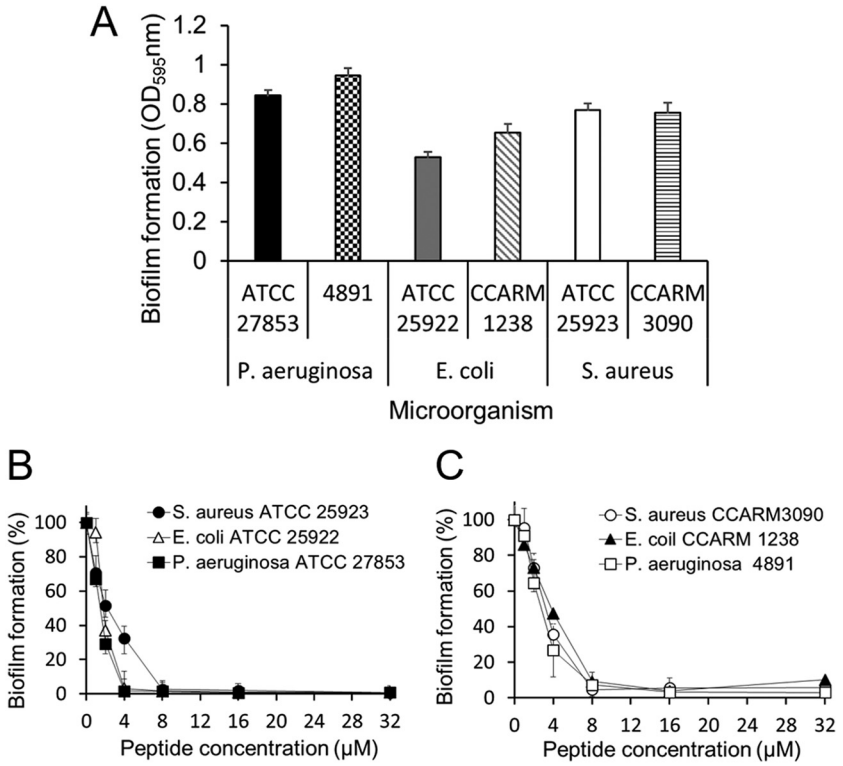

FIG 6 Inhibition of biofilm formation by Pse-T2. (A) Biofilm formation by the indicated microorganisms for 24 h at 37°C was assessed using crystal violet staining. (B and C) Effect of Pse-T2 on biofilm formation by standard bacteria (B) and MDR bacteria (C).

severely inflamed. In contrast, *P. aeruginosa* 4891-infected wounds treated with Pse-T2 at the MBIC were approximately 54% closed after 6 days and 92% closed after 10 days (Fig. 7A and Fig. 8B).

Bacterial counts were also obtained to understand the dynamics of bacterial growth on the surface of the wounds (Fig. 8A). After treatment with Pse-T2 at the MBIC, the bacterial counts were diminished by 79.7% on day 3 and by more than 95% on day 6, compared to the counts on day 0. This suggests that wound healing promoted by Pse-T2 reflects its antibacterial and antibiofilm activities.

Pse-T2 suppresses expression of proinflammatory cytokines. The mRNA expression of inflammatory mediators, such as IL-1β, IL-6, and TNF-α, is reportedly modulated

TABLE 3 Effect of the antibacterial peptide Pse-T2 on biofilm formation by various microorganisms

Microorganism	MBIC (μM)[a]	
	Pse-T2	Ciprofloxacin
Gram-positive organisms		
S. aureus ATCC 25923	8	4
S. aureus CCARM 3518	16	>400
S. aureus CCARM 3090	32	>400
Gram-negative organisms		
E. coli ATCC 25922	4	2
E. coli CCARM 1229	8	128
E. coli CCARM 1238	16	128
P. aeruginosa ATCC 27853	4	2
P. aeruginosa 4007	8	>400
P. aeruginosa 4891	16	>400

[a]Minimal biofilm inhibitory concentrations (MBICs) were determined in three independent experiments performed in triplicate.

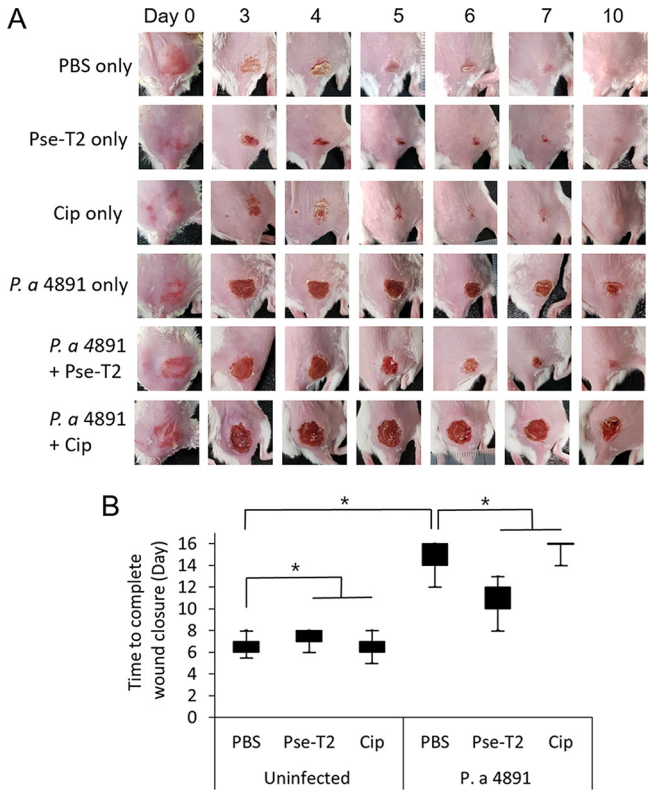

FIG 7 Effect of Pse-T2 on wound closure *in vivo*. (A) Images of wounds on days 0, 3, 4, 5, 6, 7, and 10 after injury. (B) Time to complete wound closure in each group. Data are presented as the means ± standard deviations ($n = 6$ mice per group). *, $P < 0.05$ for Pse-T2- or ciprofloxacin (Cip)-treated mice versus PBS-treated mice.

during both cutaneous infection and wound closure (Fig. 8C to E) (15). The mRNA levels of IL-1β (Fig. 8C), IL-6 (Fig. 8D), and TNF-α (Fig. 8E) were significantly upregulated within *P. aeruginosa* 4891-infected skin wounds, and this effect was inhibited by Pse-T2. In contrast, Pse-T2 had no effect on IL-1β, IL-6, and TNF-α expression within skin wounds in uninfected mice. These results indicate that Pse-T2 inhibits expression of inflammatory cytokines induced in mice by infection. Thus, Pse-T2 injection exerts antibacterial effects against *P. aeruginosa* 4891 *in vivo* and suppresses the inflammation otherwise seen in response to infection.

DISCUSSION

AMPs present in frog skin that act as agents of host defense against bacteria usually contain 12 to 48 amino acid residues (20). These peptides and the analogs derived from them are currently being investigated for their efficacy against a wide range of pathogenic and MDR bacteria. Pseudin-2 is known to have potent antimicrobial activity related to its ability to induce pore formation in bacterial cytoplasmic membranes (7, 9). Pseudin-2 has an amphipathic linear α-helical structure extending from Leu2 to Gln24 with hydrophobic side chains on one side and hydrophilic side chains on the other, which results in effective permeabilization of bacterial membranes (21). This implies that continuous amphipathic α-helicity is important for effective membrane disruption. The helical wheel projection for Pse-T2 illustrated in Fig. S1A in the supplemental material reveals that the truncated pseudin-2 analog's amphipathic helix is superior to that of pseudin-2, owing to a higher net charge, which may contribute to its enhanced antimicrobial activity. Moreover, Pse-T2 exhibits less cytotoxicity than pseudin-2 but similar antimicrobial activity against Gram-negative bacteria. These results from biological and biophysical experiments imply that Pse-T2 may have the potential to serve as a clinically useful AMP.

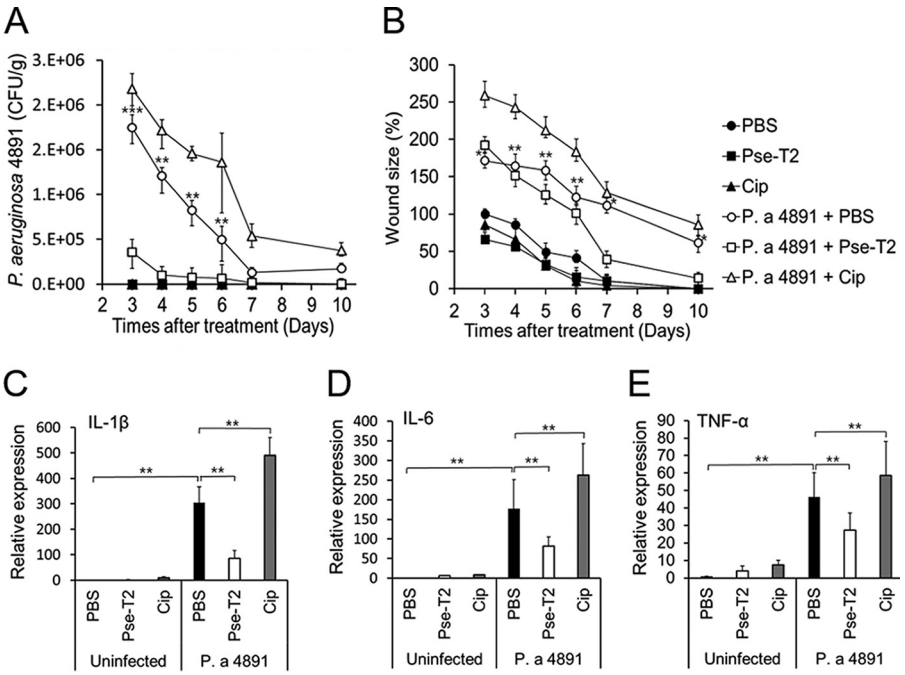

FIG 8 Effect of Pse-T2 on closure of *P. aeruginosa* 4891 (P. a 4891)-infected wounds in mice. (A) Total numbers (CFU) of *P. aeruginosa* 4891 bacteria recovered from wounds. (B) Percent change in wound size. Symbols are means ± standard deviations from three independent experiments ($n = 4$ to 6 mice per treatment group). *, $P < 0.05$; **, $P < 0.01$; ***, $P < 0.001$ (versus PBS-treated mice on day 3 after injection of *P. aeruginosa* 4891). (C to E) Relative expression levels of the indicated inflammation-related genes in wound tissues. (C) IL-1β; (D) IL-6; (E) TNF-α. Bars are means ± standard deviations from three independent experiments. **, $P < 0.01$ for Pse-T2- or ciprofloxacin (Cip)-treated mice versus PBS-treated mice.

We previously demonstrated that pseudin-2 interacts with and disrupts the *E. coli* cell membrane, causing depolarization, leakage of cellular contents, and cell death (7). Pse-T1 to -4 induced similar damage even more effectively than pseudin-2 in model bacterial membranes and the outer and inner membranes of *E. coli* (Fig. 2, Fig. 3A to C, Fig. S4, and Fig. S5). Another significant feature of the truncated pseudin-2 analogs, especially Pse-T2, is their DNA binding properties, which we detected as plasmid DNA band shifts (Fig. 3D). In contrast, pseudin-2 does not bind to DNA but was previously shown to specifically bind RNA (7). These results suggest that the truncated peptides, especially Pse-T2, disrupted the bacterial outer and inner membranes and that peptides entering the cytoplasm bind to DNA, which would be expected to inhibit protein synthesis and contribute to bacterial cell death with membrane disruption.

Biofilms are structured communities of microorganisms that are associated with surfaces and are resistant to antibiotic treatment (22, 23). Bacterial cells that are part of a biofilm are generally less susceptible to antibiotics than planktonic cells. An important factor contributing to the pathogenesis of *P. aeruginosa* is the formation of biofilms on biological surfaces, including within wounds (24, 25). Antimicrobial resistance within biofilms results in a combination of factors that include slow infiltration of antibiotics through the biofilm and induction of lipid-modifying operons by extracellular matrix DNA (24–29). We found that Pse-T2 significantly inhibited biofilm formation by *E. coli*, *P. aeruginosa*, and *S. aureus*, including their MDR strains (Fig. 6B and C and Table 3). To evaluate in the impact of Pse-T2 on wounds infected with *P. aeruginosa* 4891, we developed a model using BALB/c mice. It is known that *P. aeruginosa* is a common agent in serious infections in patients with severe wounds. Acute wounds cause a breach in the protective skin barrier and suppress the immune system, rendering patients highly susceptible to bacterial infection (13, 16). *P. aeruginosa* colonization and its rapid replication within wound tissue often lead to disseminated infections, resulting

in bacteremia, septic shock, and high rates of mortality and morbidity (16, 30). In our model, closure of *P. aeruginosa* 4891-infected skin wounds was significantly delayed compared to uninfected wounds. However, treatment of *P. aeruginosa*-infected wounds with Pse-T2 led to significant reductions in wound size along with an apparent clearance of *P. aeruginosa* 4891 biofilm from the wound. Despite the short half-life of conventional antimicrobial peptides, treatment of *P. aeruginosa* 4891-infected wounds with Pse-T2 in the early stages may result in faster wound closure and reduced inflammation because of the killing of bacteria (Fig. 8A).

Ciprofloxacin is a fluoroquinolone characterized by rapid concentration-dependent bactericidal activity against most Gram-negative bacteria (31). This antibiotic has a broad spectrum of activity and is used to treat respiratory tract infections, otitis media, sinusitis, eye infections, urinary tract infections, and sepsis (32, 33). However, a major issue associated with ciprofloxacin use, and with fluoroquinolones in general, is the development of bacterial resistance. The increasing incidence of ciprofloxacin resistance among Gram-negative bacteria has been correlated with the increasing use of fluoroquinolones (34). For example, the *P. aeruginosa* 4891 strain used in the present study is resistant to ciprofloxacin (MIC value of 400 μM or higher) (Table 2), unlike the standard strain *P. aeruginosa* ATCC 27853 (MIC value of 0.5 μM). For this reason, ciprofloxacin was used for comparison with Pse-T2 in the *in vivo* wound closure assays. Unexpectedly, treatment of *P. aeruginosa* 4891-infected wounds with ciprofloxacin led to significant increases in wound size, compared to the controls, and the wound was not healed even after 10 days (Fig. 7 and Fig. 8B). Ciprofloxacin had no hemolytic activity (Fig. S6B), indicating that the increase in wound size was not related to a toxic effect of the antibiotic. In *P. aeruginosa* 4891-infected wounds treated with ciprofloxacin, the CFU count was increased (Fig. 8A), and pus was generated around the wound area (Fig. 7A), which was not seen with the ciprofloxacin-untreated infected controls. Ciprofloxacin treatment also led to higher expression levels of genes involved in inflammation (IL-1β, IL-6, and TNF-α) within wound tissues than in controls due to the increase in wound size (Fig. 8C to E).

ndvB encodes NdvB, a glucosyltransferase required for the formation of cyclic-periplasmic glucans (35). *ndvB* expression is also important for the expression of ethanol oxidation genes, suggesting multiple roles of NdvB (36). *tssC1* is a component of the *P. aeruginosa* type VI secretion system, which is involved in biofilm-specific antibiotic resistance through an unknown mechanism (37). We assessed *ndvB* and *tssC* expression in order to determine whether the cause of the increase in wound size related to ciprofloxacin treatment was due to the expression of a *P. aeruginosa* biofilm-specific resistance gene (Table S2 and Fig. S7). We found that expression levels of both *ndvB* and *tssC* were higher in *P. aeruginosa* 4891-infected wounds treated with ciprofloxacin than in infected wounds without antibiotics. In contrast, Pse-T2 decreased *ndvB* and *tssC* expression within infected wound tissue (Fig. S7). These results indicate that ciprofloxacin promotes the expression of antibiotic resistance genes by *P. aeruginosa* 4891, which affects wound size and bacterial growth and which interferes with wound closure. In contrast, Pse-T2 does not promote resistance in this strain and thus effectively promotes wound closure. We therefore suggest that Pse-T2 warrants further study as a potential antimicrobial agent for treatment of infected wounds, particularly those infected by multidrug-resistant bacteria.

In conclusion, we investigated a set of truncated pseudin-2 analogs with linear amphipathic α-helical structures, among which Pse-T2 appears to have the most potential for clinical application. Pse-T2 showed a much greater ability to disrupt the outer/inner membrane of Gram-negative bacteria than pseudin-2 and also showed DNA binding activity. *In vivo*, Pse-T2 facilitated the healing of wounds infected by MDR *P. aeruginosa* 4891, in part by decreasing inflammation through suppression of IL-1β, IL-6, and TNF-α. All the data presented here will be helpful for the design of future AMPs for a wider array of therapeutic purposes, including infections at sites other than skin, as well as for use in biomedical materials, antibiotics, cosmetics, and antimicrobial agents.

MATERIALS AND METHODS

Ethics statement. This study conformed to the ethical standards of the Institutional Ethics Committee of Chosun University, and the protocols were approved by the Institutional Ethics Committee of Chosun University. All mouse experiments were carried out in strict accordance with National Institutes of Health guidelines for the ethical treatment of animals (43) and guidelines of the Center for Experimental Animals of Chosun University for Medical Science (permit no. CIACUC 2017-S0044).

Reagents. The following reagents were used for peptide synthesis: rink amide 4-methylbenzhydrylamine resin, *N*-hydroxybenzotriazole (HOBt), 2-(1H-benzotriazole-1-yl)-1,1,3,3-tetramethyluronium hexafluorophosphate (HBTU), 9-fluorenylmethoxy carbonyl (Fmoc)-protected amino acids (Novabiochem, Läufelfingen, Switzerland), dimethylformamide (DMF), *N*,*N*-diisopropylethylamine (DIEA), *N*-methylpyrrolidone (NMP), piperidine, trifluoroacetic acid (TFA), triisopropylsilane (TIS), and acetonitrile (Sigma-Aldrich, St. Louis, MO, USA). Calcein, fluorescein isothiocyanate (FITC), propidium iodide (PI), *n*-phenyl-1-naphthylamine (NPN), *o*-nitrophenyl-β-galactosidase (ONPG), 3,3′-dipropylthiadicarbocyanine iodide ($DiSC_3$-5), glutaraldehyde, and ciprofloxacin were purchased from Sigma-Aldrich (St. Louis, MO, USA). SYTOX green nucleic acid stain was purchased from Thermo Fisher Scientific. The following compounds were used for the production of artificial liposomes: L-α-phosphatidylethanolamine (PE), L-α-phosphatidyl-DL-glycerol sodium salt (PG), L-α-phosphatidylcholine (PC), sphingomyelin (SM), and cholesterol (CH) (Avanti Polar Lipids, Inc., Alabaster, AL, USA).

Peptide synthesis. Peptides were synthesized using the Fmoc solid-phase method on a solid support of rink amide 4-methylbenzhydrylamine resin using a Liberty microwave peptide synthesizer (CEM Co., Matthews, NC, USA). For coupling reactions, 0.1 M HOBt and 0.45 M HBTU in DMF and 2 M DIEA in NMP were used as coupling reagents, and a 10-fold excess of Fmoc-amino acid was added during all coupling cycles. Fmoc was deprotected by incubating the resin with 20% (vol/vol) piperidine in DMF. The crude peptides were repeatedly extracted with diethyl ether and then purified on a Jupiter C_{18} column (250 by 21.2 mm, 15 μM, and 300 Å) using reversed-phase preparative high-performance liquid chromatography (RP-HPLC). The molecular mass of the peptides was confirmed by using matrix-assisted laser desorption ionization (MALDI) mass spectrometry (MALDI II; Kratos Analytical, Inc., Chestnut Ridge, NY, USA).

Antimicrobial activity. Bacterial strains used in this study and their respective growth media are listed in Table S1 in the supplemental material. Five Gram-positive bacteria, including 2 MDR strains; 7 Gram-negative bacteria, including 4 MDR strains; and 2 yeast strains were used to investigate antimicrobial activity (Table S1).

To determine MICs, bacteria were incubated in culture medium overnight at 37°C. Aliquots of the bacterial cell suspension (5×10^5 CFU/ml) were then added to 96-well plates containing 2-fold serial dilutions of each peptide, and the samples were incubated at 37°C for 24 h. The lowest concentration of peptide that completely inhibited bacterial growth was deemed to be the MIC. The MICs of the peptides against the tested microorganisms were determined by using a protocol described by the Clinical and Laboratory Standards Institute (CLSI) (38).

Time-kill kinetics were assayed using *E. coli* ATCC 25922 and *S. aureus* ATCC 25923 in the presence of pseudin-2 or Pse-T1 to -4 at their respective MICs. The bacterial cells were cultured overnight until they reached the exponential growth phase and then incubated for an additional 0, 10, 20, 30, 40, 50, and 60 min at 37°C. The total bacterial population was then plated on agar plates and incubated overnight, after which the colonies were counted (7).

To assess the effect of the antibacterial peptide on biofilm formation, bacterial strains, including MDR strains (*E. coli* ATCC 25922 and CCARM 1238, *S. aureus* ATCC 25923 and CCARM 3090, and *P. aeruginosa* ATCC 27853 and 4891), were cultured in medium containing 0.2% glucose. Biofilm formation was then quantitatively analyzed as described previously (19). The MBIC was considered the lowest concentration that inhibited biofilm formation. Each measurement was performed at least three times using two replicates.

Hemolytic activity. Peptide-induced lysis of human red blood cells (hRBCs) was evaluated as follows. Fresh hRBCs were first washed 3 times through suspension in phosphate-buffered saline (PBS) followed by centrifugation for 5 min at 1,000 $\times$ *g* at 4°C. The hRBCs were then added to peptide-containing PBS (0 to 100 μM) for a final RBC concentration of 8% (vol/vol). After incubation for 1 h at 37°C, the samples were centrifuged at 1,000 $\times$ *g* for 5 min, and the absorbance of the supernatant at 414 nm was used as an index of hemolysis. As a positive control, 100% hemolysis was induced by treating hRBCs with 0.1% Triton X-100 (39). Melittin was used as a reference peptide. Three replicates were evaluated under each condition.

Cytotoxicity. MTT [3-(4,5-dimethylthiazol-2-yl)-2,5-diphenyltetrazolium bromide] assays were used to assess the cytotoxicity of each peptide against HaCaT human keratinocytes. The cells were cultured on 96-well plates to a density of 2×10^4 cells/well in Dulbecco's modified Eagle's medium (DMEM) containing 10% fetal bovine serum (FBS). Peptides were then added to various concentrations (0 to 100 μM) and incubated for an additional 24 h at 37°C, after which MTT was added to each well to a final concentration of 0.5 mg/ml and incubated for 4 h. The formazan produced was dissolved in dimethyl sulfoxide (DMSO), and the absorbance at 570 nm was measured. A 100% cytotoxic control was generated by treatment with 0.1% Triton X-100 (39). Melittin was used as a reference peptide. Three replicates were evaluated under each condition.

Circular dichroism. Peptides (40 μM) in PBS (pH 7.2) were added to a suspension of 1 mM small unilamellar vesicles composed of PE/PG (7:3, wt/wt) or PC/CH/SM (1:1:1, wt/wt/wt). CD spectra were then measured from 190 to 250 nm using a Jasco 810 spectropolarimeter (Jasco, Tokyo, Japan) (6).

AMP-induced membrane disruption. Outer membrane permeability was measured using the fluorescent dye NPN and *E. coli* cells as described previously (19). Inner membrane permeabilization in the presence of peptides was assessed by measuring β-galactosidase activity in *E. coli* using ONPG as a substrate as described previously (19). Depolarization of the cytoplasmic membrane by the peptides was detected using the membrane potential-sensitive dye $DiSC_3$-5 with intact *E. coli* and *S. aureus* cells as previously described (6).

Membrane integrity. To assess the effect of AMPs on membrane integrity, *E. coli* ATCC 25922 cells with compromised membranes after peptide treatment were detected using SYTOX green (Thermo Fisher Scientific, USA) as previously described (6). SYTOX green is a membrane-impermeant dye that becomes fluorescent when bound to nucleic acids. The dye enters only cells with a compromised plasma membrane (40). In addition, membrane integrity was also assessed through fluorescence-activated cell sorter (FACS) analysis of *E. coli*, *S. aureus*, and *P. aeruginosa* cells exposed to PI after peptide treatment, as previously described (41).

DNA binding. DNA binding assays were performed by mixing 200 ng of bacterial plasmid pRSET A (Thermo Fisher Scientific, USA) with different concentrations of peptides in 10 mM Tris buffer (pH 8.0) containing 1 mM EDTA, 5% glycerol, 20 mM KCl, and 50 μg/ml bovine serum albumin (BSA). The mixtures were incubated for 10 min at 37°C and then electrophoresed on a 1% agarose–TAE (Tris-acetate-EDTA) gel using 1× TAE buffer, after which the gels were stained with ethidium bromide (7).

Scanning electron microscopy. *E. coli* ATCC 25922 and *S. aureus* ATCC 25923 cells in mid-log phase were suspended in PBS to an optical density at 600 nm (OD_{600}) of 0.2, after which aliquots were incubated with a peptide at its MIC for 1 h at 37°C. The control was run in the absence of peptide. After incubation, cell pellets were harvested and fixed in 2.5% glutaraldehyde overnight at 4°C, followed by two washes in PBS. The fixed cells were dehydrated for 10 min each in a graded ethanol series (50%, 70%, 90%, and 100%) and for 15 min each in 100% ethanol and a mixture (1:1) of 100% ethanol and tertiary butanol. Finally, the specimens were dried, coated with platinum, and examined using a low-vacuum scanning electron microscope (JSM-IT300; JEOL, Japan).

Calcein release and estimation of peptide-induced pore size in artificial liposomes. Calcein-entrapped large unilamellar vesicles (LUVs) composed of PE/PG (7:3) or PC/CH/SM (1:1:1) were prepared as described previously (7). Measurements of peptide-induced membrane permeability were made based on the percentage of calcein that leaked from LUVs exposed to the peptide (42). To estimate the sizes of pores in the artificial vesicles, soluble fluorescent molecules (calcein, FD4, FD10, FD20, and FD40) served as models of cytoplasmic components. LUVs composed of PE/PG or PC/CH/SM and entrapping FD were prepared using the reverse-phase evaporation method (7).

Closure of wounds infected with MDR *P. aeruginosa*. Six- to seven-week-old BALB/c mice weighting 28 to 30 g ($n = 126$) were used in this study. The wound was produced by using sandpaper (no. 800; Daesung Abrasive Co., South Korea) to abrade the epidermis on the backs of the mice. *P. aeruginosa* 4891 (1×10^8 CFU per 20 μl in PBS) was then immediately applied to the created wound. Two hours after bacterial infection at the wound site, Pse-T2 at the MBIC in 20 μl of PBS was injected once. Control mice were instilled with 20 μl of PBS without Pse-T2 or ciprofloxacin. Ciprofloxacin was used for the antibiotic-treated control, and *P. aeruginosa* 4891-uninfected mice were used as uninfected controls. Wounds and the surrounding tissues were then harvested on days 3, 4, 5, 6, 7, and 10. The wounds were photographed at the indicated times, and wound size was determined. The harvested wound tissues were homogenized in 500 μl of sterile PBS using a tissue grinder. *P. aeruginosa* 4891 was quantified by plating serial dilutions of the homogenate on agar plates and incubating them for 24 h. Each dilution was plated in triplicate for counting.

Gene expression analysis using quantitative real-time PCR. The effect of Pse-T2 on the expression of several inflammatory genes after its administration to uninfected or infected mice was assessed. Briefly, total mRNA was isolated from the wound tissues using TRIzol reagent (Life Technologies, Waltham, MA, USA), after which cDNA was synthesized using a TOPscript cDNA synthesis kit (Enzynomics, Daejeon, South Korea). Quantitative PCR (qPCR) was carried out with TOPreal qPCR 2× premix (SYBR green) using a 7500 real-time PCR system (Applied Biosystems, Thermo Fisher Scientific, Inc., Waltham, MA, USA) and primers for the genes tested, including IL-1β, IL-6, and TNF-α. The qPCR protocol was as follows: 40 cycles of 50°C for 2 min and 95°C for 10 min, 95°C for 15 s, and 60°C for 1 min. For quantification of mRNA, transcript levels were normalized to the level of β-actin. Each sample was analyzed in triplicate.

Expression of biofilm-specific resistance genes (*ndvB* and *tssC1*) in *P. aeruginosa* 4891-infected mice was assessed using a specific set of primers. qPCR primers are listed in Table S2 in the supplemental material. The level of *rpoD* expression determined using qPCR was used as a reference standard.

Statistical analysis. All data are expressed as means ± standard deviations. Differences among groups were evaluated by using one-way analysis of variance. *P* values of <0.05 were considered statistically significant.

SUPPLEMENTAL MATERIAL

Supplemental material for this article may be found at https://doi.org/10.1128/AAC.01493-18.

SUPPLEMENTAL FILE 1, PDF file, 1.2 MB.

ACKNOWLEDGMENTS

This work was supported by a National Research Foundation of Korea (NRF) grant funded by the South Korean government (no. 2016R1A2A1A05005440; NRF-2017M3A9E4077206), a Global Research Laboratory (GRL) grant (no. NRF-2014K1A1A2064460), and an Institute for Information & Communications Technology Promotion (IITP) grant funded by the South Korean government (MSIT) (no. 2017-0-01714, Development of Antimicrobial Peptide Using Deep Learning).

REFERENCES

1. Davies J, Davies D. 2010. Origins and evolution of antibiotic resistance. Microbiol Mol Biol Rev 74:417–433. https://doi.org/10.1128/MMBR.00016-10.
2. Parkins MD, Floto RA. 2015. Emerging bacterial pathogens and changing concepts of bacterial pathogenesis in cystic fibrosis. J Cyst Fibros 14:293–304. https://doi.org/10.1016/j.jcf.2015.03.012.
3. Haney EF, Mansour SC, Hancock RE. 2017. Antimicrobial peptides: an introduction. Methods Mol Biol 1548:3–22. https://doi.org/10.1007/978-1-4939-6737-7_1.
4. Jahnsen RD, Frimodt-Møller N, Franzyk H. 2012. Antimicrobial activity of peptidomimetics against multidrug-resistant *Escherichia coli*: a comparative study of different backbones. J Med Chem 55:7253–7261. https://doi.org/10.1021/jm300820a.
5. Hancock REW, Sahl HG. 2006. Antimicrobial and host-defense peptides as new anti-infective therapeutic strategies. Nat Biotechnol 24:1551–1557. https://doi.org/10.1038/nbt1267.
6. Lee JK, Seo CH, Luchian T, Park Y. 2016. Antimicrobial peptide CMA3 derived from the CA-MA hybrid peptide: antibacterial and anti-inflammatory activities with low cytotoxicity and mechanism of action in *Escherichia coli*. Antimicrob Agents Chemother 60:495–506. https://doi.org/10.1128/AAC.01998-15.
7. Park SC, Kim JY, Jeong C, Yoo S, Hahm KS, Park Y. 2011. A plausible mode of action of pseudin-2, an antimicrobial peptide from *Pseudis paradoxa*. Biochim Biophys Acta 1808:171–182. https://doi.org/10.1016/j.bbamem.2010.08.023.
8. Conlon JM, Sonnevend A, Davidson C, Smith DD, Nielsen PF. 2004. The ascaphins: a family of antimicrobial peptides from the skin secretions of the most primitive extant frog, Ascaphus truei. Biochem Biophys Res Commun 320:170–175. https://doi.org/10.1016/j.bbrc.2004.05.141.
9. Pal T, Sonnevend A, Galadari S, Conlon JM. 2005. Design of potent, non-toxic antimicrobial agents based upon the structure of the frog skin peptide, pseudin-2. Regul Pept 129:85–91. https://doi.org/10.1016/j.regpep.2005.01.015.
10. Abdel-Wahab YH, Power GJ, Ng MT, Flatt PR, Conlon JM. 2008. Insulin-releasing properties of the frog skin peptide pseudin-2 and its [Lys18]-substituted analogue. Biol Chem 389:143–148. https://doi.org/10.1515/BC.2008.018.
11. Jeon D, Jeong MC, Jacob B, Bang JK, Kim EH, Cheong C, Jung ID, Park Y, Kim Y. 2017. Investigation of cationicity and structure of pseudin-2 analogues for enhanced bacterial selectivity and anti-inflammatory activity. Sci Rep 7:1455. https://doi.org/10.1038/s41598-017-01474-0.
12. Liu Y, Zhou Q, Wang Y, Liu Z, Dong M, Wang Y, Li X, Hu D. 2014. Negative pressure wound therapy decreases mortality in a murine model of burn-wound sepsis involving *Pseudomonas aeruginosa* infection. PLoS One 9:e90494. https://doi.org/10.1371/journal.pone.0090494.
13. Bjarnsholt T, Kirketerp-Møller K, Jensen PØ, Madsen KG, Phipps R, Krogfelt K, Høiby N, Givskov M. 2008. Why chronic wounds will not heal: a novel hypothesis. Wound Repair Regen 16:2–10. https://doi.org/10.1111/j.1524-475X.2007.00283.x.
14. Goldufsky J, Wood SJ, Jayaraman V, Majdobeh O, Chen L, Qin S, Zhang C, DiPietro LA, Shafikhani SH. 2015. *Pseudomonas aeruginosa* uses T3SS to inhibit diabetic wound healing. Wound Repair Regen 23:557–564. https://doi.org/10.1111/wrr.12310.
15. Han HM, Ko S, Cheong MJ, Bang JK, Seo CH, Luchian T, Park Y. 2017. Myxinidin2 and myxinidin3 suppress inflammatory responses through STAT3 and MAPKs to promote wound healing. Oncotarget 8:87582–87597. https://doi.org/10.18632/oncotarget.20908.
16. Kanno E, Kawakami K, Miyairi S, Tanno H, Suzuki A, Kamimatsuno R, Takagi N, Miyasaka T, Ishii K, Gotoh N, Maruyama R, Tachi M. 2016. Promotion of acute-phase skin wound healing by *Pseudomonas aeruginosa* C4-HSL. Int Wound J 13:1325–1335. https://doi.org/10.1111/iwj.12523.
17. Tsuchido T, Aoki I, Takano M. 1989. Interaction of the fluorescent dye 1-N-phenylnaphthylamine with *Escherichia coli* cells during heat stress and recovery from heat stress. J Gen Microbiol 135:1941–1947. https://doi.org/10.1099/00221287-135-7-1941.
18. Imura Y, Choda N, Matsuzaki K. 2008. Magainin 2 in action: distinct modes of membrane permeabilization in living bacterial and mammalian cells. Biophys J 95:5757–5765. https://doi.org/10.1529/biophysj.108.133488.
19. Han HM, Gopal R, Park Y. 2016. Design and membrane-disruption mechanism of charge-enriched AMPs exhibiting cell selectivity, high-salt resistance, and anti-biofilm properties. Amino Acids 48:505–522. https://doi.org/10.1007/s00726-015-2104-0.
20. Olson L, III, Soto AM, Knoop FC, Conlon JM. 2001. Pseudin-2: an antimicrobial peptide with low hemolytic activity from the skin of the paradoxical frog. Biochem Biophys Res Commun 288:1001–1005. https://doi.org/10.1006/bbrc.2001.5884.
21. Morris AL, MacArthur MW, Hutchinson EG, Thornton JM. 1992. Stereochemical quality of protein structure coordinates. Proteins 12:345–364. https://doi.org/10.1002/prot.340120407.
22. Reffuveille F, de la Fuente-Núñez C, Mansour S, Hancock REW. 2014. A broad-spectrum antibiofilm peptide enhances antibiotic action against bacterial biofilms. Antimicrob Agents Chemother 58:5363–5371. https://doi.org/10.1128/AAC.03163-14.
23. de la Fuente-Núñez C, Reffuveille F, Fernández L, Hancock REW. 2013. Bacterial biofilm development as a multicellular adaptation: antibiotic resistance and new therapeutic strategies. Curr Opin Microbiol 16:580–589. https://doi.org/10.1016/j.mib.2013.06.013.
24. Mah TF, Pitts B, Pellock B, Walker GC, Stewart PS, O'Toole GA. 2003. A genetic basis for *Pseudomonas aeruginosa* biofilm antibiotic resistance. Nature 426:306–310. https://doi.org/10.1038/nature02122.
25. Heydari S, Eftekhar F. 2015. Biofilm formation and beta-lactamase production in burn isolates of *Pseudomonas aeruginosa*. Jundishapur J Microbiol 8:e15514. https://doi.org/10.5812/jjm.15514.
26. Zhang L, Fritsch M, Hammond L, Landreville R, Slatculescu C, Colavita A, Mah TF. 2013. Identification of genes involved in *Pseudomonas aeruginosa* biofilm-specific resistance to antibiotics. PLoS One 8:e61625. https://doi.org/10.1371/journal.pone.0061625.
27. Mulcahy H, Charron-Mazenod L, Lewenza S. 2008. Extracellular DNA chelates cations and induces antibiotic resistance in *Pseudomonas aeruginosa* biofilms. PLoS Pathog 4:e1000213. https://doi.org/10.1371/journal.ppat.1000213.
28. Lewis K. 2008. Multidrug tolerance of biofilms and persister cells. Curr Top Microbiol Immunol 322:107–131.
29. Saffari M, Karami S, Firoozeh F, Sehat M. 2017. Evaluation of biofilm-specific antimicrobial resistance genes in *Pseudomonas aeruginosa* isolates in Farabi Hospital. J Med Microbiol 66:905–909. https://doi.org/10.1099/jmm.0.000521.
30. Deonarine K, Panelli MC, Stashower ME, Jin P, Smith K, Slade HB, Norwood C, Wang E, Marincola FM, Stroncek DF. 2007. Gene expression profiling of cutaneous wound healing. J Transl Med 5:11. https://doi.org/10.1186/1479-5876-5-11.
31. Reis AC, Santos SR, Souza SC, Saldanha MG, Pitanga TN, Oliveira RR. 2016. Ciprofloxacin resistance pattern among bacteria isolated from patients with community-acquired urinary tract infection. Rev Inst Med Trop Sao Paulo 58:53. https://doi.org/10.1590/S1678-9946201658053.
32. Dryden MS. 2010. Complicated skin and soft tissue infection. J Antimicrob Chemother 65:35–44. https://doi.org/10.1093/jac/dkq302.
33. Pea F, Crapis M, Cojutti P, Bassetti M. 2014. Daptomycin underexposure

in a young intravenous drug user who was affected by life-threatening *Staphylococcus aureus*-complicated skin and soft tissue infection associated with bacteraemia. Infection 42:207–210. https://doi.org/10.1007/s15010-013-0511-2.
34. Fair RJ, Tor Y. 2014. Antibiotics and bacterial resistance in the 21st century. Perspect Medicin Chem 6:25–64. https://doi.org/10.4137/PMC.S14459.
35. Sadovskaya I, Vinogradov E, Li JJ, Hachani A, Kowalska K, Filloux A. 2010. High-level antibiotic resistance in *Pseudomonas aeruginosa* biofilm: the *ndvB* gene is involved in the production of highly glycerol-phosphorylated beta-(1→3)-glucans, which bind aminoglycosides. Glycobiology 20:895–904. https://doi.org/10.1093/glycob/cwq047.
36. Beaudoin T, Zhang L, Hinz AJ, Parr CJ, Mah TF. 2012. The biofilm-specific antibiotic resistance gene *ndvB* is important for expression of ethanol oxidation genes in *Pseudomonas aeruginosa* biofilms. J Bacteriol 194:3128–3136. https://doi.org/10.1128/JB.06178-11.
37. Hauser AR. 2009. The type III secretion system of *Pseudomonas aeruginosa*: infection by injection. Nat Rev Microbiol 7:654–665. https://doi.org/10.1038/nrmicro2199.
38. Clinical and Laboratory Standards Institute. 2018. Performance standards for antimicrobial susceptibility testing; M100S, 28th ed. Clinical and Laboratory Standards Institute, Wayne, PA.
39. Lee JK, Park SC, Hahm KS, Park Y. 2013. Antimicrobial HPA3NT3 peptide analogs: placement of aromatic rings and positive charges are key determinants for cell selectivity and mechanism of action. Biochim Biophys Acta 1828:443–454. https://doi.org/10.1016/j.bbamem.2012.09.005.
40. Roth BL, Poot M, Yue ST, Millard PJ. 1997. Bacterial viability and antibiotic susceptibility testing with SYTOX green nucleic acid stain. Appl Environ Microbiol 63:2421–2431.
41. Zhu X, Zhang L, Wang J, Ma Z, Xu W, Li J, Shan A. 2015. Characterization of antimicrobial activity and mechanisms of low amphipathic peptides with different alpha-helical propensity. Acta Biomater 18:155–167. https://doi.org/10.1016/j.actbio.2015.02.023.
42. Sun CS, Wang CY, Chen BP, He RY, Liu GC, Wang CH, Chen W, Chern Y, Huang JJ. 2014. The influence of pathological mutations and proline substitutions in TDP-43 glycine-rich peptides on its amyloid properties and cellular toxicity. PLoS One 9:e103644. https://doi.org/10.1371/journal.pone.0103644.
43. National Research Council. 2011. Guide for the care and use of laboratory animals, 8th ed. The National Academies Press, Washington, DC.